

Defect engineering of p-type silicon heterojunction solar cells fabricated using commercial-grade low-lifetime silicon wafers

Daniel Chen¹ | Moonyong Kim¹ | Jianwei Shi² | Bruno Vicari Stefani¹ | Zhengshan (Jason) Yu² | Shaoyang Liu¹ | Roland Einhaus³ | Stuart Wenham¹ | Zachary Holman² | Brett Hallam¹

¹School of Photovoltaic and Renewable Energy Engineering, University of New South Wales, Kensington, NSW, 2052, Australia

²School of Electrical, Computer and Energy Engineering, Arizona State University, Tempe, AZ, 85287

³Apollon Solar, Charlemagne, Lyon, 69002, France

Correspondence

Daniel Chen, School of Photovoltaic and Renewable Energy Engineering, The University of New South Wales, Kensington, NSW 2052, Australia.

Email: daniel.chen@unsw.edu.au

Funding information

Australian Academy of Science, Grant/Award Number: J.G Russell prize; Australian Centre for Advanced Photovoltaics, Grant/Award Numbers: 1-SRI00, 1-SRI001; Institution of Engineering and Technology, Grant/Award Number: AF Harvey Engineering Prize; Australian Government Research Training Program, Grant/Award Number: RSAP1000; Australian Renewable Energy Agency, Grant/Award Number: RND005; Australian Research Council, Grant/Award Number: DE170100620; National Science Foundation and the Department of Energy Cooperative Agreement, Grant/Award Number: EEC-1041895

Abstract

In this work, we integrate defect engineering methods of gettering and hydrogenation into silicon heterojunction solar cells fabricated using low-lifetime commercial-grade p-type Czochralski-grown monocrystalline and high-performance multicrystalline wafers. We independently assess the impact of gettering on the removal of bulk impurities such as iron as well as the impact of hydrogenation on the passivation of grain boundaries and B-O defects. Furthermore, we report for the first time the susceptibility of heterojunction devices to light- and elevated temperature-induced degradation and investigate the onset of such degradation during device fabrication. Lastly, we demonstrate solar cells with independently verified 1-sun open-circuit voltages of 707 and 702 mV on monocrystalline and multicrystalline silicon wafers, respectively, with a starting bulk minority-carrier lifetime below 40 microseconds. These remarkably high open-circuit voltages reveal the potential of inexpensive low-lifetime p-type silicon wafers for making devices with efficiencies without needing to shift towards n-type substrates.

KEY WORDS

boron-oxygen defect, gettering, hydrogenation, LeTID, p-type, silicon heterojunction solar cell

1 | INTRODUCTION

The silicon heterojunction (SHJ) solar cell owes its success to the excellent passivation quality provided by hydrogenated amorphous silicon (a-Si:H) films.¹ These films have enabled devices with open-circuit voltages (V_{oc}) over 750 mV and multiple efficiency demonstrations beyond 25%,^{2–4} with the current world record of 26.7%.⁵ In addition to the excellent surface passivation, SHJ cells have

been attributed manufacturing advantages, where devices can be (and, in fact, must be) completely fabricated below 250°C.⁶ Such temperature restrictions prevent both a degradation of the a-Si:H passivation layers and degradation of the bulk silicon material commonly associated with higher-temperature processing.^{7,8} These lower temperatures also enable the simple fabrication of symmetrical bifacial structures and the use of thinner wafers without thermal-stress-related yield losses.⁹ However, to take full

This is an open access article under the terms of the Creative Commons Attribution License, which permits use, distribution and reproduction in any medium, provided the original work is properly cited.

© 2019 The Authors. Progress in Photovoltaics: Research and Applications published by John Wiley & Sons Ltd

TABLE 1 Published J-V performance metrics of leading n-type and p-type silicon heterojunction solar cells from various research groups and SHJ manufacturers

Affiliation	η , %	V _{OC} , mV	J _{SC} , mA/cm ²	FF, %	Material	Area, cm ²	Status	Year
n-type								
Kaneka, ³ Japan	26.7	738	42.7	84.9	Cz	79.0	IC	2017
Panasonic, ² Japan	25.6	740	41.8	82.7	Cz	143.7	IC	2014
Hanergy, China	25.11	747	39.5	85.0	Cz	244.45	IC	2019
SHARP Corporation, ¹⁰ Japan	25.1	736	41.7	81.9	Cz	3.72	IC	2014
Meyer Burger/CSEM, ¹¹ Switzerland	25.0	740	41.7	80.9	Cz	90.25	IC	2019
CEA-INES, ¹² France	24.4	738	40.0	82.6	Cz	222.1	IC	2019
Meyer Burger, ¹³ Germany	24.26	739	39.8	82.4	Cz	244.32	-	2019
EPFL, ¹⁴ Switzerland	24.1	727	40.8	81.1	Fz	4	IC	2018
CIC, ¹⁵ Japan	24.1	745	38.8	83.2	Cz	243.4	PR	2016
Chengdu Zhufeng Yongming Technology, ¹⁶ China	23.9	740	39.1	82.6	Cz	-	-	2019
Hevel Solar, ¹⁷ Russia	23.04	735	38.7	81.0	Cz	244	PR	2018
QEERI/EPFL/CSEM, ¹⁸ Qatar/Switzerland	22.2	723	39.4	77.6	QM	4.03	IC	2019
p-type								
EPFL, ¹⁴ Switzerland	23.8	722	40.7	80.7	FZ	4	IC	2018
EPFL, Switzerland	23.6	739	39.6	80.8	Cz	-	IC	2018
QEERI/EPFL/CSEM, ¹⁸ Qatar/Switzerland	22.6	725	39.4	79.1	QM	4.03	IC	2019
Meyer Burger, ¹⁹ Switzerland	20.7	728	37.5	75.7	Cz	239	-	2016
UNSW/ASU, ²⁰ Australia/USA	18.7	691	36.2	74.4	MC	4	PR	2019
ENEA, ²¹ Italy	17.6	710	33.4	74.1	FZ	4	PR	2017

Abbreviations: QM, quasi-mono; FZ, float zone; MC, multicrystalline; IC, independently confirmed; PR, peer-reviewed publication.

advantage of the excellent efficiency capabilities of SHJ cells, high-lifetime silicon wafers are required. Table 1 lists several recently fabricated SHJ devices on n-type and p-type silicon wafers as an extension to the technology summary presented by De Wolf et al.⁶ Remarkably, although n-type SHJ technologies have continuously pushed the limits of efficiency beyond 25%, the performance of p-type SHJ has yet to see such breakthroughs and is still well behind the UNSW 25%-efficient, 706-mV p-type PERL solar cell fabricated over two decades ago,²² and the more recent 26.1% (V_{OC} of 737 mV) polycrystalline silicon on oxide (POLO) interdigitated back contact (IBC) cell by ISFH.²³ Nonetheless, significant progress has been made in 2018 with the fabrication of a 23.8%-efficient device.¹⁴ It is also interesting to note that there is little work in recent years in the area of multicrystalline silicon (mc-Si) solar cells using SHJ technologies. In contrast, optimisation of other passivation techniques such as those used in p-type passivated emitter and rear cell (PERC) solar cells and n-type tunnel oxide passivated contact (TOPCon) solar cells has enabled mc-Si devices with efficiencies reaching 22.04% (V_{OC} of 672 mV) and 22.3% (V_{OC} of 674 mV), respectively.^{24,25} Although SHJ devices are more commonly fabricated on n-type substrates, p-type materials, in particular mc-Si, still offer a competitive cost advantage when it comes to ingot production. If these lower quality substrates can be transformed into high-efficiency devices, then there exists a chance for a low-cost and commercially competitive option. Fundamental

studies are critical to understanding the potential of such materials and suitability for next-generation solar cells featuring carrier-selective contacts.

1.1 | Defects and degradation in p-type silicon

A common pitfall of p-type silicon is the increased susceptibility of the material to recombination-active defects within the bulk.^{26,27} Metallic impurities (including iron, copper, titanium, nickel, and cobalt)²⁶ and other point defects introduced from the silicon feedstock can be found in high concentrations in both Czochralski-grown (Cz) and mc-Si p-type wafers (eg, interstitial oxygen concentration $[O_i] \approx 10^{17}/\text{cm}^3$ and substitutional carbon concentrations $[C_s] > 10^{17}/\text{cm}^3$ ²⁸). Due to the charge state of defects and their position within the band-gap, interstitial iron (Fe_i), for example, even in small concentrations ($< 10^{11}/\text{cm}^3$), can result in large reductions in final cell efficiency.²⁹ Fe_i and copper (Cu) concentrations are also commonly used as metrics to assess the efficiency of gettering processes.³⁰ This is due to their relatively simple detection methods and high diffusivity and therefore responsiveness to gettering processes.³¹ On the other hand, studies on industrial PERC solar cells have shown that metals such as copper, nickel, and cobalt are more detrimental to device performance in n-type silicon than in p-type silicon for similar impurities concentrations.²⁶ Mc-Si wafers have both a larger concentration of metallic impurities and inherently

high densities of crystallographic and structural defects such as dislocation clusters and grain boundaries, further reducing device performance. The efficiency of devices such as SHJ solar cells should have a greater sensitivity to these defects as other forms of recombination become less dominant.

Another significant obstacle encountered by p-type materials is carrier- and light-induced degradation.^{32,33} For example, boron-oxygen (B-O) related defects, which form predominantly in p-type Cz silicon wafers in the presence of carrier injection, have been shown to result in up to 2% absolute drop in efficiency under standard operating conditions in the field.³⁴ On a similar note, a newly emerging light- and elevated temperature-induced degradation (LeTID) mechanism has been observed to affect all types of silicon materials (n-type and p-type, Cz, mc-Si, and float-zoned [FZ] silicon^{35–38}) and is particularly severe in p-type mc-Si wafers. Petter et al³⁹ reported a 16% relative drop in efficiency on p-type mc-Si PERC solar cells in the field. Although the exact configuration or source of the recombination activity is yet to be identified, numerous studies have postulated hydrogen as a possible root cause.^{37,40,41} An interesting observation by Chan et al^{37,41} and in our previous work is the manifestation of LeTID during annealing at elevated temperatures (between 150°C and 250°C) in the dark.

1.2 | Gettering, hydrogenation, and the importance of high temperatures

Although p-type silicon wafers are subject to low starting lifetimes, defect engineering processes such as gettering and hydrogenation have long demonstrated an impressive ability to enhance their lifetime.⁴² The use of gettering and hydrogenation is widespread in the production of conventional aluminium back surface field (Al-BSF) and PERC silicon solar cells. However, the use of these methods on other solar cells, in particular SHJ cells, for the elimination of bulk defects is less prominent.

Gettering is particularly effective for the removal of fast-diffusing lifetime-limiting bulk impurities.^{30,43,44} It is usually done externally via phosphorus diffusion gettering (PDG) during emitter formation. Conventional PDG relies on the movement of mobile species towards heavily diffused getter sites near the surface. A subsequent emitter etch-back may then be used to remove these impurities from the substrate. In addition, internal gettering, such as the precipitation and/or the migration of Fe_i to defective regions (eg, grain boundaries and dislocations in mc-Si) under these thermal conditions, can also be a viable method of impurity isolation.

Similarly, hydrogen is well known for the passivation of bulk impurities and crystallographic defects in silicon.^{45–47} In conventional commercial solar cells, hydrogen-containing dielectric layers such as hydrogenated silicon nitride (SiN_x:H) and hydrogenated aluminium oxide (AlO_x:H) are deposited using plasma-enhanced chemical vapour deposition (PECVD) to provide excellent surface passivation for silicon wafers. During subsequent thermal treatment, such as metallisation co-firing, hydrogen from these layers is incorporated into the silicon, passivating the surface interface region as well as diffusing

throughout the bulk silicon to defect sites.^{47–49} Particularly in mc-Si wafers, hydrogenation processes have been shown to significantly reduce the recombination activity at grain boundaries and dislocation clusters, with Martinuzzi et al^{47,48} observing an 80% increase in minority-carrier diffusion length after hydrogenation. Furthermore, subsequent thermal processes with hydrogen present, performed in conjunction with carrier injection via illumination or current injection, have also demonstrated benefits for bulk defect passivation. In particular, these processes can permanently deactivate the B-O defect in boron-doped Cz silicon wafers.^{50–52} Conventional methods of B-O deactivation involved illuminated annealing with intensities between 0.5 and 3 suns at temperatures of 50°C to 230°C for durations beyond 2 hours.⁵³ Recent developments at UNSW with the advanced hydrogenation process (AHP) have accelerated B-O deactivation by rapidly controlling the charge state of bulk interstitial hydrogen previously released from the SiN_x:H coatings.^{45,54} Hallam et al⁴⁸ reported deactivation using 360°C for 8 seconds with an illumination intensity of ≈160 sun. The injection of carriers using illumination increases the generation of the highly mobile neutral charge species (H⁰), as well as the minority species (H⁻ in p-type silicon) and accelerates defect formation.^{45,55} A combination of these species provides a form of rapid transport of hydrogen throughout the silicon bulk and a passivation of positively charged defects such as B-O.⁴⁹ In addition, high-intensity illumination pushes the silicon into high-injection conditions, accelerating the formation of the B-O defect. The increased availability of formed defects also accelerates hydrogenation, thus enabling full passivation of B-O defects in under 10 seconds.⁴⁸

A key component of both the gettering and hydrogenation mechanisms is diffusivity, and this has important implications for SHJ cells processed at low temperatures. Consider, for example, gettering of fast-diffusing Fe_i: Figure 1A shows the time taken for Fe_i to diffuse through 100 μm of silicon—approximately half the thickness of a wafer. Note that the diffusion time *t* is calculated according to $t = (L_D)^2/D$ where *L_D* is the diffusion length and *D* is the diffusivity of the mobile species extracted from.⁶⁷ At temperature of 800°C, which are commonly experienced by silicon wafers during emitter diffusion, Fe_i diffusion can be achieved in under 4 minutes, whereas at SHJ processing temperatures of around 250°C, over 110 hours is required. Not only is this too slow for production, which typically requires a throughput of over 3600 wafers per hour, but the transport of Fe_i within the substrate may also have complications that further increase the required time. This includes, for example, the stifling of Fe_i diffusion over time into regions already saturated with high Fe_i concentrations.

Similarly, bulk passivation with hydrogen is extremely temperature dependent. Figure 1B shows a compilation of temperature-dependent hydrogen diffusivity data in monocrystalline and multicrystalline silicon, converted into the time required to diffuse through 100 μm. An extrapolation of the data from Van Wieringen and Warmoltz⁸² (blue line) is often considered as an upper limit for hydrogen diffusivity, presumably corresponding to a majority of the hydrogen either in the neutral (H⁰) charge state or without significant interaction with traps in lightly doped material.

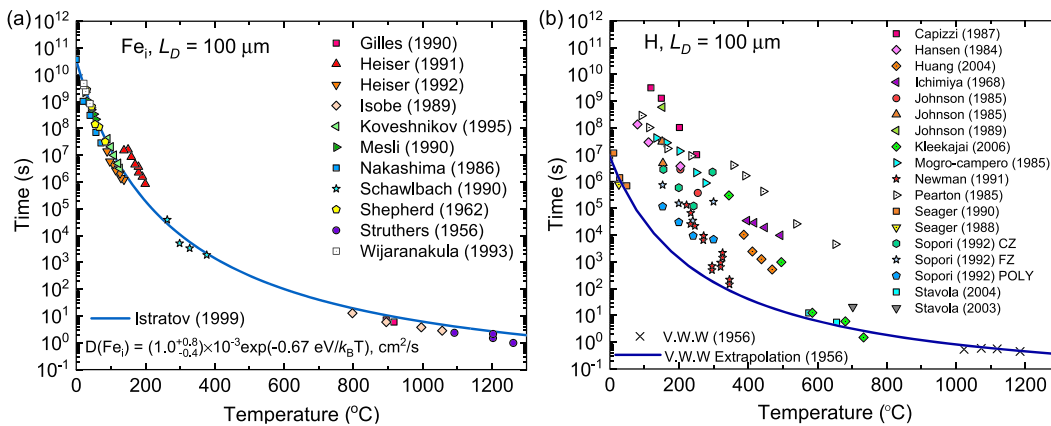


FIGURE 1 Calculated time, as a function of temperature, required for the diffusion of (A) Fe_i and (B) hydrogen through $L_D = 100 \mu\text{m}$ of crystalline silicon. Diffusivity data for Fe_i were extracted from previous studies.^{56–66} The solid blue line represents the extrapolation of Fe_i diffusivity presented Istratov et al.⁶⁷ Hydrogen diffusivity data were taken from other works.^{68–81} The solid purple line represents the extrapolation of the hydrogen diffusivity from the work of Van Wieringen and Warmoltz (diffusion coefficient reported as $D = 9.4 \times 10^{-3} \exp(-\frac{11000}{RT}) \text{ cm}^2/\text{s}$; where R is the universal gas constant)⁸²

If we again consider the process parameters for the AHP described by Hallam et al.,⁴⁸ a 360°C process for 8 seconds would correspond to an upper-limit diffusion length for hydrogen of $L_D = 34 \mu\text{m}$, insufficient for the distribution of hydrogen throughout the bulk. SHJ device processing temperatures around 250°C would require at least 5 to 10 minutes for hydrogen to diffuse $100 \mu\text{m}$ from the surface into the bulk, and hydrogen diffusivity is often of orders of magnitude lower than the upper limit used to calculate this time. In the vicinity of 250°C , the measured diffusivity of hydrogen varies by approximately four orders of magnitude, and the highest experimentally determined diffusivity is more than an order of magnitude lower than the Van Wieringen and Warmoltz extrapolation. For this condition, durations of up to 3 hours may be required to achieve a diffusion length of $100 \mu\text{m}$. The diffusivity of hydrogen also heavily depends on the charge state of hydrogen,⁸³ which is controlled by the material's background doping, temperature, and excess carrier concentration.⁸⁴ The migration of hydrogen is often limited by interactions with traps (particularly in mc-Si), especially at low temperatures, and therefore affected by the concentration of impurities and defects in the material, further reducing diffusivity.^{85,86} For effective passivation in an SHJ solar cell, it is desirable for hydrogen to be dispersed throughout the bulk of the wafer prior to AHP.

One method of achieving this would be to use initial higher-temperature processing steps, such as an equivalent conventional metallisation firing step, to introduce hydrogen into the bulk prior to SHJ fabrication. To obtain a hydrogen diffusion length of $100 \mu\text{m}$ in less than 10 seconds, a timescale compatible with high-throughput manufacturing, a temperature in excess of 500°C is required. Experimental data within the temperature range of 600°C to 800°C measured by Kleekajai et al.⁶⁸ match closely with predicted upper limits. We may thus expect that, under standard solar cell firing conditions, temperatures above 730°C will enable hydrogen to diffuse throughout a silicon wafer within 3 seconds. These temperatures and timescales have been demonstrated to be correlated with the passivation

of grain boundaries in mc-Si wafers during conventional firing processes, therefore providing evidence for the diffusion of hydrogen throughout the wafer.^{42,87}

1.3 | Defect engineering of silicon heterojunction solar cells

The use of defect engineering for SHJ solar cells has already demonstrated promising results. Park et al.⁸⁸ investigated the impact of PDG prior to SHJ cell fabrication, resulting in >20 mV improvements in final device V_{OC} . In our previous work, we applied both prefabrication hydrogenation and gettering treatments on SHJ cells and cell precursors fabricated on p-type Cz wafers, achieving a V_{OC} of 692 mV and enhancements of over 70 mV when compared with cells without pretreatment.⁸⁹ Basnet et al.⁹⁰ combined tabula rasa and PDG processes on n-type upgraded metallurgical grade (UMG) silicon material, demonstrating impressive iV_{OC} of 723 mV on lifetime structures and an efficiency of 21.2% (V_{OC} of 718 mV) on finished cells. Haschke et al.⁹¹ applied hydrogenation and gettering treatments to n-type quasi-mono wafers, achieving V_{OCs} beyond 720 mV and an efficiency of 21.5%.

In this work, we apply various pre- and post-fabrication defect engineering treatments on p-type SHJ solar cells. We further extend the work in Hallam et al.⁸⁹ through incorporation of the UNSW AHP, demonstrating independently confirmed enhancements in V_{OC} to beyond 700 mV on both p-type Cz and mc-Si SHJ solar cells. We then discuss the significance of defect engineering in the removal of iron, the enhancement of bulk minority-carrier lifetime, and the suppression of B-O-related light-induced degradation in SHJ structures. Lastly, we demonstrate the susceptibility of SHJ solar cells to LeTID for the first time, indicating that the conventional process flow for SHJ solar cell fabrication may cause such degradation in hydrogenated samples.

2 | METHODOLOGY

2.1 | Defect engineering of p-type wafers

To highlight the potential of performance-enhancing defect engineering processes, we used low-lifetime wafers typically used for the fabrication of commercial-grade solar cells. P-type 156 mm × 156 mm Cz silicon wafers with a resistivity of $1.6 \pm 0.2 \Omega \text{ cm}$ and pre-textured, high-performance mc-Si wafers with a resistivity of $1.8 \pm 0.2 \Omega \text{ cm}$ were acquired from LONGi Solar and GCL Energy Holdings, respectively. Adjacent samples or "sister" sets were chosen as references for both groups to minimise discrepancy in electronic or crystallographic quality between wafers. Cz wafers were first alkaline etched in sodium hydroxide (NaOH) (30% v/v) solution to remove saw damage. Mc-Si wafers did not undergo any initial saw damage removal process as the wafers were pre-textured by the supplier and the alkaline process would result in an undesirable polishing effect. All wafers were then allocated into four primary groups of 12 wafers each: a control set without any defect engineering prefabrication treatment (Control), a prefabrication hydrogenated group (H), a prefabrication gettered group (G), and a final group with both pre-fabrication hydrogenation and gettering treatments (G + H). Any samples undergoing elevated temperatures or contamination-sensitive processing were chemically cleaned using the Radio Corporation of America (RCA) 1 and two processes: a 6-minute submersion in a mixture of ammonium hydroxide (NH_4OH) and hydrogen peroxide (H_2O_2), a rinse in deionised water (DIW), and a 6-minute ionic clean in a solution of 37% hydrochloric acid (HCl) and H_2O_2 heated to 75°C. This was followed by a short dip in dilute 2% hydrofluoric acid (HF) to remove any oxides present on the surface.

The gettering treatment was achieved by phosphorus diffusion in a quartz tube furnace with a phosphoryl chloride (POCl_3) source, resulting in dual-sided n⁺-emitters with sheet resistances of $35 \pm 2 \Omega/\text{sq}$. This diffusion is a single-step process at an approximate temperature of 840°C for 45 minutes, with an O₂ flow of 150 sccm, an N₂ flow of 6 slm, and a POCl_3 flow of 600 sccm. A short dip in 2% HF for 2 minutes was used to remove the surface phosphosilicate glass layer. To remove diffused layers and ensure similar wafer thicknesses, all wafers, including those in the control groups, were alkaline and acidic textured for Cz and mc-Si wafers, respectively, removing approximately 10 μm off each side and resulting in a final substrate thickness of $180 \pm 4 \mu\text{m}$. For the hydrogenation treatment, 75 nm of hydrogenated SiN_x:H was first deposited on both sides of each wafer using a Meyer Burger MAiA remote plasma-enhanced chemical vapour deposition (r-PECVD) tool directly after RCA cleaning. Deposited wafers were then annealed at a temperature of $740 \pm 6^\circ\text{C}$ using a Schmid fast-firing metallisation belt furnace at a constant belt speed of 4.5 m/min to allow for the release of hydrogen from the dielectric layers and diffusion throughout the silicon. Actual wafer temperatures were measured on identically processed wafers using a Q13 Datapaq temperature profiler averaged using three Omega KMQXL-IM075G-300 K-type thermocouples. Dielectric layers were then removed using a solution of

dilute 2% (v/v) HF at room temperature until wafers were hydrophobic.

2.2 | P-type heterojunction solar cell fabrication

Prior to the fabrication of SHJ solar cell precursors, all wafers were again chemically cleaned. This three-step cleaning process consisted of (a) a Piranha clean for 10 minutes in a 4:1 ratio of 96% sulfuric acid (H_2SO_4) and H_2O_2 heated to 110°C followed by a 10-minute rinse in DIW, (b) a 10-minute RCA 2 clean, and (c) a 1-minute submersion in 10:1 buffered oxide etch (BOE) followed by a 10-minute rinse in DIW. A 6-nm-thick intrinsic a-Si:H(i) layer was deposited on the rear surface using a mixture of silane and hydrogen precursor gases in an Applied Materials P-5000 multi-chamber direct PECVD tool. This was immediately followed by a deposition of an 11-nm-thick boron-doped a-Si:H (p) film through the addition of trimethylboron dopant gas. The same tool was then used to deposit an identical 6-nm-thick intrinsic a-Si:H (i) layer on the front surface, followed by a 5-nm-thick phosphorus-doped a-Si:H(n) film by adding phosphine dopant gas. Note that an in situ 30 seconds hydrogen plasma treatment at 250°C was performed directly after a-Si:H(i) deposition (on both sides) to improve the passivation quality at the a-Si:H(i)/c-Si interface.^{92,93} Some of these wafers were then removed for characterisation as lifetime test structures whereas others were fabricated into cells. Figure 2 depicts the fabrication flow for SHJ lifetime test structures and full SHJ solar cells.

For the fabrication of full SHJ cells, 75 nm of indium tin oxide (ITO) was deposited on the front side using an MRC-944 direct current magnetron sputtering tool. A 150-nm-thick ITO layer and 200-nm-thick silver electrode were then sputtered on the rear side using the same tool. A shadow mask was used to define four $2 \times 2 \text{ cm}^2$ solar cells during both front and rear side sputtering processes. Subsequently, a front silver grid pattern consisting of low-temperature silver paste was screen printed on the front side. A paste-curing process at 200°C for 20 minutes was conducted to finish this front electrode. These cells were then cut from the 156-mm substrate using a 1064-nm Nd:YAG laser. After characterisation, the UNSW AHP incorporating minority-carrier injection was applied to further enhance passivation of bulk defects such as the B-O defect and to suppress any LID.^{48,51,94} This process was performed on a hot plate operating at 300°C with the temperature of the wafers monitored in-situ using an infrared thermometer (PC301HT-0, Calex). A fibre-coupled diode laser with a wavelength of 938 nm operating in quasi-continuous mode (0.5 ms pulse length with a repetition frequency of 2 kHz) was used to illuminate the samples at >100 suns for a period of 10 seconds. Testing for B-O defect passivation and stability was carried out using a 0.02 kW/m² white-light LED for a period of 48 hours at room temperature ($23 \pm 2^\circ\text{C}$).

2.3 | Characterisation

Lifetime testing was performed using quasi-steady-state photoconductance (QSSPC) measurements (WCT-120, Sinton Instruments) with analysis performed using the generalised method^{95,96} and

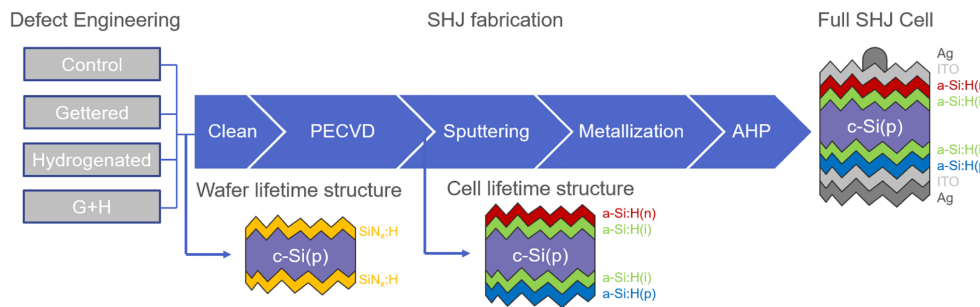


FIGURE 2 Process flow diagram for the fabrication of defect-engineered p-type SHJ lifetime structures and solar cells

corrected for intrinsic and Auger recombination using a parameterisation method proposed by Richter et al.⁹⁷ The minority-carrier effective lifetime (τ_{eff}) was extracted at a minority-carrier injection level of $\Delta n = 1 \times 10^{15}/\text{cm}^3$ or approximately 0.1 of the background dopant concentration, generally to allow for comparison between wafers with different resistivities without the influence of the dopant concentration.⁹⁸ Bulk minority-carrier lifetimes (τ_{bulk}) were extracted at $\Delta n = 1 \times 10^{15}/\text{cm}^3$ after excluding the surface-related lifetime component (determined using the Kane-Swanson method⁹⁹) from the inverse Auger corrected lifetime.¹⁰⁰ Lifetime characterisation was carried out after deposition of $\text{SiN}_x:\text{H}$ dielectric layers, after firing and after application of (intrinsic and doped) a-Si:H films. Fe_i concentrations ([Fe_i]) were extracted from lifetime structures through the method described in Macdonald et al.³¹ Iron-boron pairs (FeB) were dissociated into Fe_i through a 10-second light soak under approximately 2 kW/m² illumination (measured using a PM100D power metre and a S350C thermal power sensor [Thorlabs]) from a broad-band halogen light source. The substrates were removed from light exposure periodically to prevent heating which may drive the reverse association reactions. The lifetime prior to light soaking was measured after the samples were left in dark storage for at least 3 hours at room temperature,¹⁰¹ to allow for the complete association of FeB pairs. [Fe_i] was then extracted at a minority-carrier injection level of $\Delta n = 1 \times 10^{15}/\text{cm}^3$ in order to operate away from the cross-over point.³¹ Photoluminescence (PL) images acquired from a BTImaging LIS-R3 tool provided a spatially resolved assessment of the substrate quality. These images were taken at 1-sun illumination with an exposure duration of 0.1 second and were calibrated using the method described in Hallam et al¹⁰² to yield implied-V_{OC} (iV_{OC}) maps. In order to correct for photon smearing, the images were deconvoluted via means of a point spread function¹⁰³ using a MATLAB-based software PLPro embedded within the LumiTools software suite.¹⁰⁴ Initial current-voltage (I-V) characteristics were measured in-house under standard testing conditions: steady-state illumination intensity of 0.1 W/cm² with an AM1.5G spectrum and a temperature of 25°C. Error ranges in Tables 2 and 3 account for uncertainties in the area, systematic errors, and fluctuations in the steady-state illumination. We note that the reference sample used to calibrate the sample was a PERC solar cell whereas a SHJ solar cell would have been more ideal to account for spectral mismatch. V_{OCS} of the champion cells within the G + H groups were independently verified by the Solar Energy Research Institute of Singapore (SERIS) at the National University of Singapore

(Reference cell traceability: Serial Number—016-2014, Certificate number—1016-2014109ISE).

3 | RESULTS AND DISCUSSION

3.1 | Defect-engineered silicon heterojunction solar cells

3.1.1 | P-type monocrystalline silicon

The [Fe_i], bulk minority-carrier lifetime, and iV_{OC} measured on $\text{SiN}_x:\text{H}$ -passivated p-type Cz silicon substrates are presented in Figure 3. Gettering significantly reduces [Fe_i] by nearly two orders of magnitude from an average concentration of approximately [Fe_i] = $3 \times 10^{11}/\text{cm}^3$ to [Fe_i] = $5 \times 10^9/\text{cm}^3$ (see Figure 3A). Hydrogenation produces a marginal drop in the [Fe_i] to [Fe_i] = $1.3 \times 10^{11}/\text{cm}^3$, which may be attributed to gettering via the $\text{SiN}_x:\text{H}$ dielectric layers or the hydrogen passivation of Fe_i during firing.^{105–107} Figure 3A also indicates that, for the gettered samples, a subsequent hydrogenation step through firing resulted in an increase in [Fe_i]. We believe that this may be due to the dissolution of precipitated iron back into interstitial form at higher temperatures as described by Lelievre et al.¹⁰⁸ Similar concentrations in Fe_i (not shown) were extracted for SHJ precursors after the removal of $\text{SiN}_x:\text{H}$ layers and deposition of a-Si:H films. Nonetheless, the enhancements from defect engineering are reflected in the respective increases in both the bulk minority-carrier lifetime (Figure 3B) and the iV_{OC} (Figure 3C). By using both gettering and hydrogenation processes in conjunction with each other, we can achieve a sevenfold increase in τ_{bulk} and a maximum iV_{OC} measured above 700 mV.

The injection-dependent minority-carrier lifetime of subsequently fabricated SHJ precursors in each processing group are shown in Figure 4. On control samples without any pretreatment, the effective lifetime is low, at $\tau_{\text{eff}} = 20 \mu\text{s}$. This translates to a low iV_{OC} of 620 mV. With hydrogenation alone, a value of $\tau_{\text{eff}} = 35 \mu\text{s}$ is measured, which may be due to the hydrogen passivation of any defects present within the bulk. Fitting of the injection-dependent Shockley-Read-Hall (SRH) components of the lifetime curves (not shown) reveals the existence of an SRH defect with a capture cross-section ratio σ_n/σ_p of approximately 14 and 16 for the control and hydrogenated samples, respectively, raising the possibility of B-O-related defect activation

TABLE 2 Performance of best p-type Cz SHJ solar cells fabricated on substrates with various defect-engineering treatments, before and after AHP on the same cells

Process Group	J_{SC} , mA/cm ²	V_{OC} , mV	FF, %	η , %
Control	33.3 (+1.8/-1.7)	621 (± 0.1)	68.9 (± 0.2)	14.2 (+0.8/-0.8)
H	34.7 (+1.9/-1.7)	628 (± 0.1)	66.4 (± 0.2)	14.5 (+0.8/-0.8)
G	34.4 (+1.9/-1.7)	643 (± 0.1)	68.9 (± 0.2)	15.2 (+0.9/-0.8)
G + H	34.5 (+1.9/-1.7)	693 (± 0.1)	69.6 (± 0.2)	16.6 (+1.0/-0.9)
Control + AHP	34.6 (+1.9/-1.7)	630 (± 0.1)	66.3 (± 0.2)	14.5 (+0.8/-0.8)
H + AHP	33.4 (+1.8/-1.7)	635 (± 0.1)	70.0 (± 0.2)	14.8 (+0.9/-0.8)
G + AHP	34.2 (+1.8/-1.7)	673 (± 0.1)	67.9 (± 0.2)	15.6 (+0.9/-0.8)
G + H + AHP	34.6 (+1.9/-1.7) (34.3 ^a)	707 (± 0.1) (707 ^a)	72.1 (± 0.3) (74.1 ^a)	17.6 (+1.0/-0.9) (18.0 ^a)

Note. I-V measurements were performed in-house at UNSW.

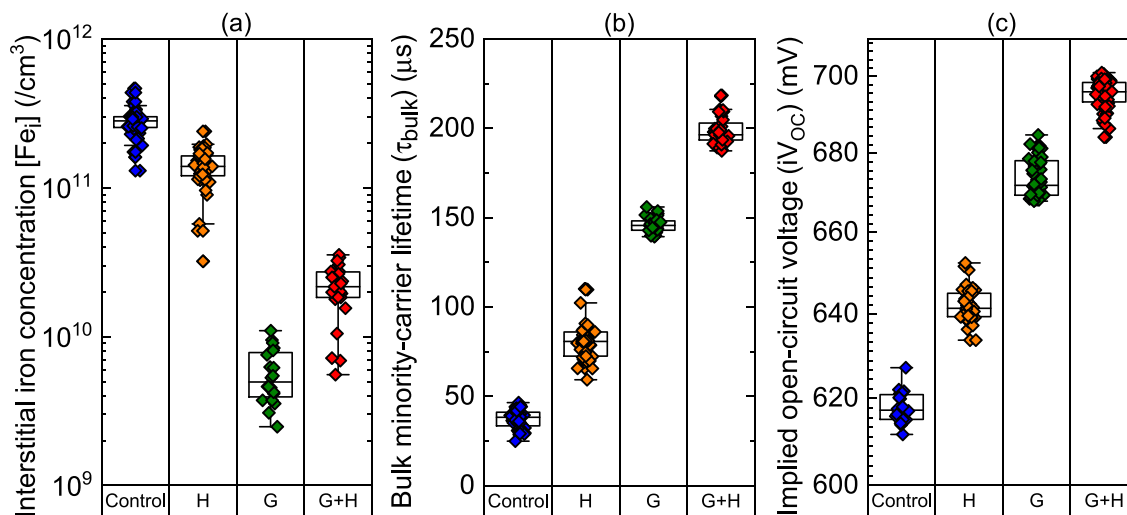
^aIndependently measured at SERIS.

TABLE 3 Performance of best p-type mc-Si SHJ solar cells fabricated on substrates with various defect-engineering treatments, before and after AHP on the same cells

Process Group	J_{SC} , mA/cm ²	V_{OC} , mV	FF, %	η , %
Control	31.9 (+1.8/-1.6)	632 (± 0.1)	61.1 (± 0.2)	12.3 (+0.7/-0.7)
H	31.2 (+1.7/-1.6)	636 (± 0.1)	66.9 (± 0.2)	13.3 (+0.8/-0.7)
G	33.5 (+1.9/-1.7)	683 (± 0.1)	63.4 (± 0.2)	14.5 (+0.9/-0.8)
G + H	32.1 (+1.8/-1.6)	657 (± 0.1)	68.6 (± 0.2)	14.5 (+0.9/-0.8)
Control + AHP	35.1 (+2.0/-1.8)	640 (± 0.1)	62.9 (± 0.2)	14.1 (+0.8/-0.8)
H + AHP	33.6 (+1.9/-1.7)	685 (± 0.1)	67.9 (± 0.2)	15.6 (+0.9/-0.9)
G + AHP	33.0 (+1.8/-1.7)	687 (± 0.1)	68.9 (± 0.2)	15.6 (+0.9/-0.9)
G + H + AHP	34.9 (+1.9/-1.8) (19.6 ^a)	701 (± 0.1) (702 ^a)	70.6 (± 0.2) (72.1 ^a)	17.3 (+1.0/-0.9) (9.9 ^a)

Note. I-V measurements were performed in-house at UNSW. Note that the champion cell had sustained damage prior to independent verification such that the exact cell area and hence J_{SC} could not be accurately determined.

^aIndependently measured at SERIS.

**FIGURE 3** (A) Fe_i concentration, (B) bulk minority-carrier lifetime, and (C) IV_{Oc} taken from SiNx:H-passivated precursor substrates after undergoing no defect engineering treatments (control), hydrogenation treatment (H), gettering treatment (G), or both gettering and hydrogenation treatments (G + H). Bulk minority-carrier lifetime and iron concentrations were extracted at an injection level of $\Delta n = 1 \times 10^{15}/\text{cm}^3$

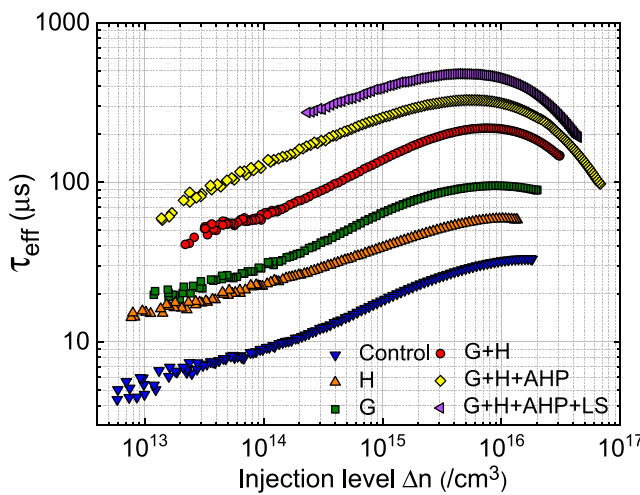


FIGURE 4 Injection-dependent minority-carrier lifetime measured on Cz SHJ cell precursors after undergoing no defect engineering treatments (control), hydrogenation treatment (H), gettering treatment (G), or both gettering and hydrogenation treatments (G + H). Further included are the lifetimes after AHP (G + H + AHP) and the subsequent LID stability testing (G + H + AHP + LS)

(the sensitivity of these wafers to B-O degradation was assessed on identically gettered wafers in another experiment, which demonstrated a 41%_{rel} drop in τ_{eff} from 76 to 46 μs).³² This would not be unexpected in p-type wafers, which may have been exposed to illumination between SHJ fabrication processes and characterisation. Samples that received only a gettering treatment achieved a threefold gain in τ_{eff} to 67 μs , resulting in an iV_{OC} of 653 mV. Upon using both gettering and hydrogenation treatments, the bulk carrier lifetime improves sevenfold to $\tau_{\text{eff}} = 215 \mu\text{s}$, yielding an iV_{OC} of up to 687 mV, already at or slightly above the V_{OC} of commercially produced p-type PERC cells.¹⁰⁹ Although the carrier lifetimes measured on these wafers are far below what can already be achieved on existing commercial PERC and Al-BSF structures using similar p-type wafers, we find that they are limited by B-O-related bulk degradation. By subsequently applying the AHP laser treatment for B-O deactivation, we observe a further enhancement in carrier lifetime of the G + H sample to $\tau_{\text{eff}} = 305 \mu\text{s}$ with an iV_{OC} of 705 mV. After subsequent stability testing at 1-sun for 48 hours, we find that the lifetime further increases beyond 390 μs ($iV_{\text{OC}} = 715 \text{ mV}$). Although this behaviour is usually not expected for p-type Cz wafers passivated using $\text{SiN}_x:\text{H}$ undergoing identical testing, enhancements in interface passivation from a-Si:H films under illumination have been reported.^{110,111} Koyabashi et al observed a 60% enhancement in the τ_{eff} of i-p/i-n a-Si:H passivated n-type lifetime structures after light soaking under 1-sun with a temperature of $32 \pm 2^\circ\text{C}$ for up to 85 hours. A close inspection of their results after 48 hours depicts an approximate improvement of 30%, which is consistent with our observed enhancements albeit on p-type wafers. We also find that although the low-injection, B-O-related SRH behaviour is no longer present after AHP and after stability testing, we continue to observe injection-

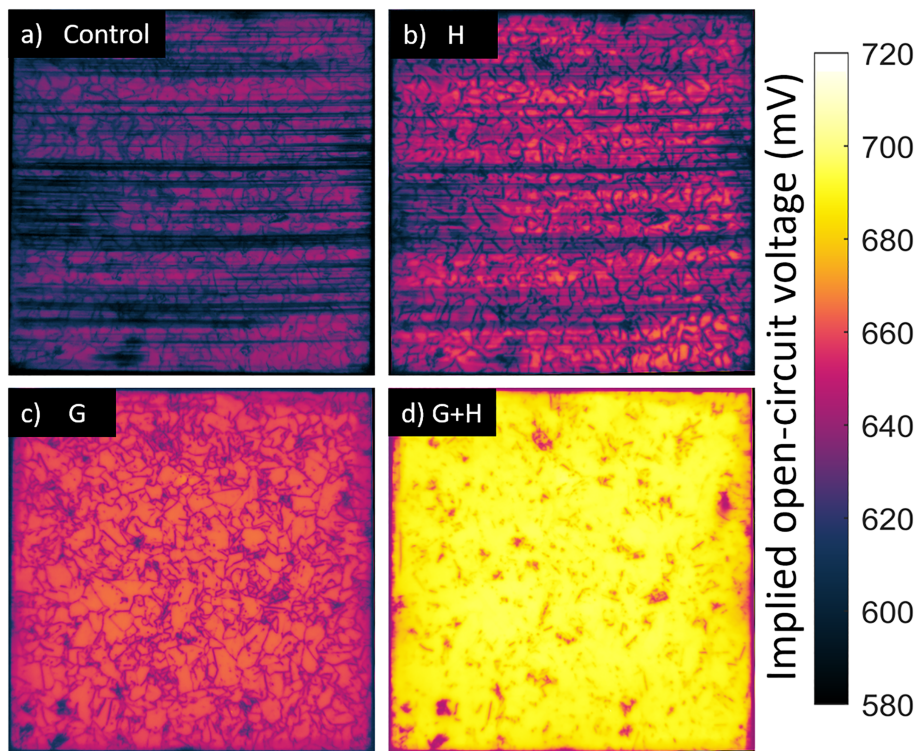
dependent recombination activity that cannot be accurately explained using SRH defect parameters. This behaviour is similar to that observed in previous studies,^{5,6,112} which was postulated to be due to surface-assisted minority-carrier recombination. Later analysis by Olibet et al¹¹³ suggested a possible involvement of dangling bonds at the a-Si:H/c-Si interface which occurs more predominantly on p-type substrates than on n-type substrates. Similar low-injection recombination activity was observed by Adachi et al⁴ on SHJ structures fabricated on n-type substrates; however, the reduction in low-injection lifetime is believed to be more pronounced on p-type substrates.¹¹² Regardless, this residual recombination provides potential for further defect passivation in future work.

A summary of the device performance of the best cell in each group before and after the AHP is presented in Table 2. We find that the trend in finished cells prior to the laser process corresponds closely with the lifetime behaviour in the cell precursor test structures. The AHP improves V_{OC} by up to 30 and 15 mV within the G and G + H groups up to 673 and 707 mV, respectively. This voltage of 707 mV was independently confirmed at SERIS, thus exceeding the V_{OC} measured on the UNSW record p-type PERL cell fabricated on a FZ substrate.²² Control and H groups were also enhanced by 9 and 7 mV to 630 and 635 mV, respectively. We note that the efficiencies reported are low due to a poor FF (66%-72%). A comparison of the light J-V and Suns- V_{OC} curves indicated a series resistance (R_s) of 7.7 $\Omega\cdot\text{cm}^2$ and 6.5 $\Omega\cdot\text{cm}^2$ on the champion cell prior to and after AHP. We speculate that this may be due to a combination of resistive losses both in the a-Si:H films and the low temperature cured paste. We cannot, however, exclude other factors such as laser-edge-isolation which may also affect both the J_{SC} and FF.

3.1.2 | P-type multicrystalline silicon

In agreement with the results on Cz wafers, gettering and hydrogenation provide similar benefits for mc-Si wafers. The PL images in Figure 5 were measured directly after $\text{SiN}_x:\text{H}$ deposition and high-temperature firing. As seen in the control sample (Figure 5A), without treatment, the lifetime is limited by saw damage and grain boundaries with a spatially averaged iV_{OC} of 615 mV. Hydrogenation (Figure 5B) results in slight improvement within intra-grain regions but little change at grain boundaries, raising the iV_{OC} to an average of 625 mV. Similar behaviours within the intra-grain regions are observed with gettering, with additional removal or passivation of the saw-damage (Figure 5C), thus realising an average iV_{OC} of 660 mV. Since all samples were etched back identical amounts, regardless of whether they received a phosphorous diffusion, we may rule out that the saw damage was removed through chemical etching. Gettering and hydrogenation processes together (Figure 5D) enhance passivation of the intra-grain areas and the grain boundaries, significantly beyond what is achieved by each process individually. Impressively, we are able to measure an averaged iV_{OC} of 700 mV across all wafers in this group, despite the control samples suggesting the presence of saw damage. The large disparity in improvement between the two hydrogenated

FIGURE 5 Calibrated iV_{OC} maps of $\text{SiN}_x\text{-H}$ passivated mc-Si wafers after undergoing no defect engineering treatments (control), hydrogenation treatment (H), gettering treatment (G), or both gettering and hydrogenation treatments (G + H)



groups (H and G + H) is of interest, as it appears that gettered samples respond more to the effects of hydrogenation. On nongettered wafers, there may be an inadequate concentration of bulk hydrogen to passivate the crystal defects sufficiently, or perhaps a redistribution of mobile impurities during firing.¹¹⁴ The enhanced hydrogen passivation after gettering may be due to the reduction in bulk impurities and defect states thus reducing the need for significant quantities of hydrogen in order to passivate remaining recombination-active constituents. However, an equally likely explanation is that some impurities that may be effectively gettered may not be effectively hydrogen passivated.

As with the Cz wafers, performance improvements were observed on fabricated cells in response to the AHP. The performances of the best p-type mc-Si cells in each group before and after the AHP are presented in Table 3. An improvement in V_{OC} of up to 44 mV was observed within the G + H + AHP group, with a maximum V_{OC} of 701 mV (independently measured at SERIS to be 702 mV). Impressively, this is approximately 30 mV higher than the V_{OC} for record efficiency devices on both n-type and p-type mc-Si.^{24,115}

However, we find an intriguing observation in the V_{OC} behaviour prior to AHP that differs from the trends observed on $\text{SiN}_x\text{-H}$ passivated samples: on average, the G + H group demonstrated a V_{OC} more than 20 mV lower than the G group. A difference in 26 mV is seen from the best cells in each group. We suspect that the observed lower V_{OC} may have been influenced by LeTID, which will be discussed in Section 3.3.

3.2 | Hydrogen passivation of B-O defects in p-type Cz SHJs

Elimination of the B-O defect in p-type Cz silicon is essential for maintaining the performance of solar cells. In Section 3.1, we discussed the impacts of the AHP in enhancing bulk passivation within both Cz and mc-Si silicon wafers after hydrogenation. Figure 6 shows

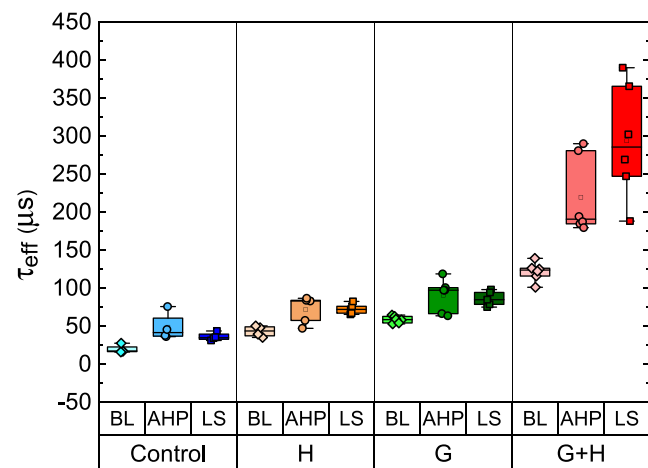


FIGURE 6 τ_{eff} of Cz SHJ cell precursors measured before AHP laser processing (BL), after AHP laser processing (AHP) and after additional light soaking for 48 hours at room temperature (LS) to check for stability. Lifetimes were extracted at an excess carrier concentration $\Delta n = 1 \times 10^{15}/\text{cm}^3$

the effects of AHP on the permanent deactivation of B-O and stability under illumination. Consistent with the V_{OC} s in Table 2, the minority-carrier lifetime of samples in all groups increase, most plausibly due to the dissociation or passivation of pre-existing B-O defects and/or the passivation of other defects. Stability testing of the samples for 48 hours under illumination at room temperature yielded interesting results: Although the stability of the hydrogenated samples (H and G + H groups) may be expected, samples in all groups—including those without hydrogenation (Control and G groups)—also demonstrated stable lifetime. Fitting of lifetime curves from C and G groups (not shown) reveals that they no longer exhibit B-O-related SRH recombination. One possible explanation is that hydrogen passivation of the B-O defect is occurring in all samples during AHP in the presence of a-Si:H passivating films. A second possible explanation is that hydrogen is introduced during the a-Si:H(i) deposition process which includes a 30 second H_2 plasma treatment step at 250°C. This phenomena was also observed in our prior work looking at the passivation of B-O defects in SHJ solar cells fabricated on compensated n-type silicon wafers.¹¹⁶ Follow-up work determined that the plasma hydrogenation step, in addition to the lowering of the Si-H bond rupture energy through deposition of the a-Si:H(p) layer, both lead to an increased concentration of H injected into the bulk.¹¹⁷

Further work will be required to determine which of these explanations may or may not be responsible for the behaviour in Figure 6.

3.3 | Hydrogen-related degradation in mc-Si SHJs

In Section 3.1, we suggested that hydrogenated SHJ solar cells may be susceptible to LeTID as an explanation for the lower-than-expected V_{OC} s measured directly after fabrication. We observed this phenomenon only on hydrogenated wafers (groups H and G + H), in agreement

with recent studies proposing hydrogen as a root cause for LeTID.^{37,41,118–120} Chan et al reported that LeTID can occur in the dark at elevated temperatures, and SHJ cells undergo such process steps.^{36,41} In particular, the PECVD deposition of the a-Si:H layers and the curing of the silver paste front electrode are usually conducted at temperatures between 200°C and 250°C in the absence of illumination. From the work by Chan et al,⁴¹ at these temperatures, the estimated time to reach maximum degradation of p-type mc-Si may be as quick as 10 minutes or as slow as 50 minutes, depending on the device structure and any thermal pretreatments.

In order to investigate possible LeTID during SHJ fabrication, mc-Si G + H sister wafers from the same batch as those in Section 3.1.2 were put through a series of dummy processing steps inclusive of PECVD deposition and paste curing, interspersed with lifetime measurements. Following the hydrogenation firing step and the removal of the SiN_x :H dielectric layers, we first deposited a-Si:H (i) layers on both sides of the wafers using identical conditions to those used to fabricate finished cells. The process duration was approximately 3.25 minutes per side (6.5-minute total) at a setpoint temperature of 250°C. The wafers were then loaded into the PECVD deposition chambers to simulate the deposition of the doped layers. No precursor gases were introduced, and no plasma was generated, but the wafers sat at 250°C for 2.5 minutes (a-Si:H(n) simulation) and then for 3 minutes (a-Si:H(p) simulation). Lastly, samples were annealed on a hot plate at 200°C for 20 minutes to simulate paste curing. Figure 7A shows the minority-carrier effective lifetime measured directly after firing (passivated with SiN_x :H), subsequent to each incremental PECVD deposition or thermal treatment (passivated with a-Si:H(i)), and after curing. After each processing step, the carrier lifetime degrades, reaching up to 80% relative degradation after curing. Monitoring of the dark saturation current density (J_{OS}) after each process indicated a minimal change in the surface passivation quality, thus indicating that the degradation was due to a change in the bulk

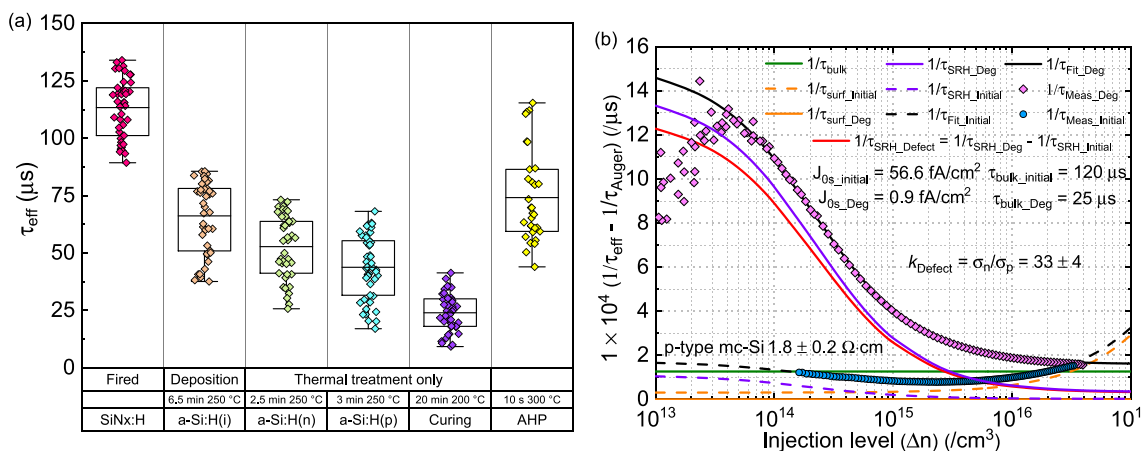


FIGURE 7 (A) Minority-carrier effective lifetime at an injection level of $\Delta n = 1 \times 10^{15}/cm^3$ of mc-Si SHJ cell precursors measured after various SHJ cell fabrication (or simulated fabrication) steps. Initial lifetimes in the first column are measured on SiN_x :H passivated samples after firing whereas the remaining lifetimes are measured with a-Si:H(i) passivation. (B) Injection-dependent inverse lifetime breakdown of SRH, bulk and surface components of a sample in its degraded state (after curing)

quality. Moreover, PL imaging (not shown) provided a qualitative spatial assessment of the samples showing a homogeneous degradation across the wafers and that the repeated handling of wafers did not compromise the passivation quality. With an additional AHP step performed after curing, the lifetime recovers slightly but not to its pre-degraded state. Treatments for B-O passivation have been shown not to be entirely effective for the treatment of LeTID in mc-Si⁹⁴; hence, further optimisation will be required to achieve complete defect mitigation.

In order to verify whether the observed degradation was in fact an onset of LeTID, we carried out injection-dependent lifetime spectroscopy analysis on the samples in their most degraded state. Figure 7B shows the inverse lifetime of one sample after firing ($1/\tau_{\text{Meas_Initial}}$) and after curing ($1/\tau_{\text{Meas_Deg}}$). A fit is used to separate out the surface lifetime components ($1/\tau_{\text{surf_Initial/Deg}}$) and the SRH lifetimes ($1/\tau_{\text{SRH_Initial/Deg}}$) from both Auger corrected inverse lifetime measurements. A defect lifetime component ($1/\tau_{\text{SRH_Defect}}$) is then derived from a linear subtraction of the two SRH lifetimes at all injection levels (ie, $1/\tau_{\text{SRH_Defect}} = 1/\tau_{\text{SRH_Deg}} - 1/\tau_{\text{SRH_Initial}}$). This subtraction allows us to exclude any defects that are intrinsic to the sample or may have formed during the firing process, assuming that any change in the bulk SRH lifetime during degradation may be due the single defect under investigation. Fitting of the $1/\tau_{\text{SRH_Defect}}$ component was carried out assuming a mid-gap defect state, as the exact energy level remains unknown and a broad range of energy levels with sufficient distance away from the band edges should produce recombination resembling that of a mid-gap defect. We identify an asymmetric electron-to-hole capture cross-section ratio $k_{\text{Defect}} = \sigma_n/\sigma_p$ of 33 ± 4 for the defect under investigation. This value matches well with the k -values associated with the defect responsible for LeTID in various other works.^{36,121,122}

Thus, we report for the first time that SHJ solar cells may also be susceptible to the LeTID degradation phenomena commonly observed in PERC solar cells and that the fabrication process flow of SHJ devices may facilitate the defect formation process. An open question is why the same LeTID phenomenon was not seen in the gettered and hydrogenated Cz solar cells and why the V_{OC} of that group was instead significantly higher than the other groups. Although Cz materials are also prone to LeTID,³⁶ this may be due to inherently lower LeTID-related precursor concentrations in Cz wafers. Unlike in Cz, the greater quantity of crystallographic defects and grain boundaries present in mc-Si may enhance hydrogen diffusivity via these alternate pathways into the bulk.⁸⁷ LeTID is also suspected to be caused by a secondary impurity (eg, metallic impurities,¹²³ vacancies,³⁷ and oxygen precipitates²⁸) that may bind to hydrogen to form a recombination active complex. This secondary impurity, the exact of which is still unknown, may be present in far lower concentrations within Cz silicon than in mc-Si. As a component of future work, LeTID in SHJ cells may be eliminated or prevented, firstly, through hydrogenation processes at lower temperatures that may be used to maintain effective hydrogen passivation without leading to subsequent degradation^{124,125} and secondly, by treating LeTID prior to SHJ processing to limit formation during cell fabrication.

4 | CONCLUSION

In this work, we incorporated prefabrication gettering and a multistage hydrogenation process into SHJ solar cells fabricated on low-quality p-type substrates with initial τ_{bulk} lower than 40 μs . Using this method, we demonstrated open-circuit voltages exceeding 700 mV for both mc-Si and Cz p-type SHJ solar cells. For mc-Si, the V_{OC} is approximately 30 mV higher than that for current record efficiency devices. Our study also identified, for the first time, the presence of LeTID in hydrogenated SHJ solar cells. The mitigation or suppression of this defect in such structures is an area that requires further investigation, particularly when using low-quality substrates that require bulk hydrogenation. The demonstration of such high V_{OC} values in this work challenges the assertion that expensive, high-quality n-type wafers are needed for fabrication of SHJ solar cells. Although the efficiencies of our initial cells are relatively low, the inherent efficiency limitation due to the bulk material causing low terminal voltages has been overcome. If the issues regarding J_{SC} and FF can be overcome, low-lifetime p-type silicon wafers could be an alternative material for the fabrication of SHJ devices and perhaps, other passivated contact solar cells.

FUNDING INFORMATION

Australian Centre for Advanced Photovoltaics (ACAP), grant number: 1-SRI001.

National Science Foundation and the Department of Energy Cooperative Agreement: No. EEC-1041895.

Australian Research Council (ARC), award number: DE170100620.

Australian Academy of Science: J. G Russell prize.

Australian Renewable Energy Agency (ARENA): RND005.

Australian Government Research Training Program: RSAP1000.

Institution of Engineering and Technology: AF Harvey Engineering Prize.

ACKNOWLEDGMENTS

The authors would like to dedicate this work to the late Professor Stuart Wenham (15 July 1957 to 23 December 2017) for his dedication and contributions to photovoltaics around the world. The views expressed herein are not necessarily the views of the Australian Government, and the Australian Government does not accept responsibility for any information or advice contained herein. The authors would also like to acknowledge Huy Duc Dao and the processing team in the Solar Industrial Research Facility at UNSW for assistance in sample fabrication and Dr Matthew Wright and William Weigand for useful discussions.

ORCID

Daniel Chen  <https://orcid.org/0000-0001-7379-4751>

Moonyong Kim  <https://orcid.org/0000-0002-3860-5633>

Bruno Vicari Stefani  <https://orcid.org/0000-0002-1307-9462>

Zhengshan (Jason) Yu  <https://orcid.org/0000-0002-4305-5912>

Shaoyang Liu  <https://orcid.org/0000-0003-4827-3828>

Zachary Holman  <https://orcid.org/0000-0002-0694-1341>

Brett Hallam  <https://orcid.org/0000-0002-4811-5240>

REFERENCES

1. Fuhs W, Niemann K, Stuke J. Heterojunctions of amorphous silicon and silicon single crystals. *Tetrahedrally Bond. Amorph Semicond Int Conf.* 1974;345(1974):345-350.
2. Masuko K, Shigematsu M, Hashiguchi T, et al. Achievement of more than 25% conversion efficiency with crystalline silicon heterojunction solar cell. *IEEE J Photovoltaics.* 2014;4(6):1433-1435.
3. Yoshikawa K, Kawasaki H, Yoshida W, et al. Silicon heterojunction solar cell with interdigitated back contacts for a photoconversion efficiency over 26%. *Nat Energy.* 2017;2(5):17032.
4. Adachi D, Hernández JL, Yamamoto K. Impact of carrier recombination on fill factor for large area heterojunction crystalline silicon solar cell with 25.1% efficiency. *Appl Phys Lett.* 2015;107(23):233506.
5. Yoshikawa K, Yoshida W, Irie T, et al. Exceeding conversion efficiency of 26% by heterojunction interdigitated back contact solar cell with thin film Si technology. *Sol Energy Mater Sol Cells.* 2017;173 (April):37-42.
6. De Wolf S, Descoeuilles A, Holman ZC, Ballif C. High-efficiency silicon heterojunction solar cells: a review. *green.* 2012;2:7-24.
7. Yano A, Tohoda S, Matsuyama K, et al. 24.7% record efficiency HIT solar cell on thin silicon wafer. *IEEE J Photovoltaics.* 2014;4(1):96-99.
8. Macdonald D, Cheung A, Cuevas A. Gettering and poisoning of silicon wafers by phosphorus diffused layers. *3rd World Conf on Photovoltaic Energy Conversion, 2003 Proc.* 2003;2:11-14.
9. Herasimenka SY, Dauksher WJ, Boccard M, Bowden S. ITO/SiO_x:H stacks for silicon heterojunction solar cells. *Sol Energy Mater Sol Cells.* 2016;158:98-101.
10. Nakamura J, Asano N, Hieda T, Okamoto C, Katayama H, Nakamura K. Development of heterojunction back contact Si solar cells. *IEEE J Photovoltaics.* 2014;4(6):1491-1495.
11. Lachenal D, Papet P, Legradic B, et al. Optimization of tunnel-junction IBC solar cells based on a series resistance model. *Sol Energy Mater Sol Cells.* 2019;200(June):110036.
12. Jouini, A. (2019) The road from recent records to the PV industry adoption for competitive LCOE Cast Mono and SHJ. *SNEC Int. Photovolt. Power Gener. Smart Energy Exhib. Conf.*
13. Vetter, E., Zhao, J., König, M., Burger, M., Gmbh, G., and Baumschule, A. Der (2019) Pilot production of bifacial Meyer Burger Heterojunction cells and modules as well as test field results. *2019 IEEE 46th Photovolt. Spec. Conf. PVSC 2019.*
14. Ballif C, Boccard M, Despesse M. The amazing improvement of silicon heterojunction technology: ready for a true mass market launch. *2018 IEEE 7th World Conf Photovoltaic Energy Conversion, WCPEC 2018 - A Jt Conf 45th IEEE PVSC, 28th PVSEC 34th EU PVSEC.* 2018;2104-2107.
15. Kobayashi E, Watabe Y, Yamamoto T, Yamada Y. Cerium oxide and hydrogen co-doped indium oxide films for high-efficiency silicon heterojunction solar cells. *Sol Energy Mater Sol Cells.* 2016;149: 75-80.
16. Peng, C., Lei, C., Ruan, T., Zhong, J., Yang, M., Long, W., Yu, C., Li, Y., and Xu, X. (2019) High phosphorus-doped seed layer in microcrystalline silicon oxide front contact layers for silicon heterojunction solar cells. *IEEE 46th Photovolt. Spec. Conf. PVSC 2019.*
17. Terukov, E., Kosarev, A., Abramov, A., and Malchukova, E. (2018) From 11% thin film to 23% heterojunction technology (HJT) PV cell: research, development and implementation related 1600 × 1000 mm² PV modules in industrial production, in *Solar Panels and Photovoltaic Materials*, InTech, pp. 13.
18. Kivambe MM, Haschke J, Horzel J, et al. Record-efficiency n-type and high-efficiency p-type monolike silicon heterojunction solar cells with a high-temperature gettering process. *ACS Appl Energy Mater.* 2019;2(7):4900-4906.
19. Batzner, D.L., Andretta, L., Frammelsberger, W., Kramer, R., Lachenal, D., Legradic, B., Meixenberger, J., Paper, P., Strahm, B., Wahli, G., Habermann, D., Frigge, S., and Sperlich, H. (2016) Bifacial p-type solar cells exhibiting low temperature coefficients: heterojunction technology. *32nd Eur. Photovolt. Sol. Energy Conf. Exhib.*, 1-10.
20. Vicari Stefani B, Weigand W, Wright M, et al. P-type upgraded metallurgical-grade multicrystalline silicon heterojunction solar cells with open-circuit voltages over 690 mV. *Phys status solidi.* 2019;216(17):1900319.
21. Mercaldo LV, Bobeico E, Usatii I, et al. Potentials of mixed-phase doped layers in p-type Si heterojunction solar cells with ZnO:Al. *Sol Energy Mater Sol Cells.* 2017;169:113-121.
22. Green MA. The path to 25% silicon solar cell efficiency: History of silicon cell evolution. *Prog Photovoltaics Res Appl.* 2009;17(3): 183-189.
23. Haase F, Hollemann C, Schäfer S, et al. Laser contact openings for local poly-Si-metal contacts enabling 26.1%-efficient POLO-IBC solar cells. *Sol Energy Mater Sol Cells.* 2018;186(May):184-193.
24. JinkoSolar P-type Multi-crystalline Silicon Solar Cells Achieve New World Record in Conversion Efficiency Again. https://www.jinkosolar.com/press_detail_1380.html.
25. Benick J, Richter A, Muller R, et al. High-efficiency n-type HP mc silicon solar cells. *IEEE J Photovoltaics.* 2017;7(5):1171-1175.
26. Schmidt J, Lim B, Walter D, et al. Impurity-related limitations of next-generation industrial silicon solar cells. *IEEE J Photovoltaics.* 2013;3(1):114-118.
27. Seibt, M., and Kveder, V. (2012) Gettering processes and the role of extended defects, in *Advanced Silicon Materials for Photovoltaic Applications*, pp. 127-188.
28. Wagner M, Wolny F, Hentsche M, et al. Correlation of the LeTID amplitude to the aluminium bulk concentration and oxygen precipitation in PERC solar cells. *Sol Energy Mater Sol Cells.* 2018;187(June): 176-188.
29. Abbott MD, Poplavskyy D, Scardera G, et al. Iron contamination in silicon solar cell production environments. *2014 IEEE 40th Photovolt Spec Conf.* 2014;3479-3484.
30. Phang SP, Macdonald D. Boron, phosphorus and aluminum gettering of iron in crystalline silicon: experiments and modelling. *Conf Rec IEEE Photovolt Spec Conf.* 2010;352-356.
31. Macdonald DH, Geerligs LJ, Azzizi A. Iron detection in crystalline silicon by carrier lifetime measurements for arbitrary injection and doping. *J Appl Phys.* 2004;95(3):1021-1028.
32. Bothe K, Schmidt J. Electronically activated boron-oxygen-related recombination centers in crystalline silicon. *J Appl Phys.* 2006;99(1): 013701.
33. Ramspeck K, Zimmermann S, Nagel H, et al. Light induced degradation of rear passivated mc-Si solar cells. *Proc 27th Eur Photovolt Sol Energy Conf.* 2012;1:861-865.
34. Knobloch J, Glunz SW, Biro D, Warta W, Schaffer E, Wetting W. Solar cells with efficiencies above 21% processed from Czochroalski grown silicon. *Proc 25th IEEE Photovolt Spec Conf Washington, DC IEEE.* 1996;405-408.
35. Fertig F, Lantzsch R, Mohr A, et al. Mass production of p-type Cz silicon solar cells approaching average stable conversion efficiencies of 22 %. *Energy Procedia.* 2017;124:338-345.
36. Chen D, Kim M, Stefani BV, et al. Evidence of an identical firing-activated carrier-induced defect in monocrystalline and multicrystalline silicon. *Sol Energy Mater Sol Cells.* 2017;172(June): 293-300.
37. Chen D, Hamer PG, Kim M, et al. Hydrogen induced degradation: a possible mechanism for light- and elevated temperature- induced

- degradation in n-type silicon. *Sol Energy Mater Sol Cells*. 2018;185:174-182.
38. Niewelt T, Selinger M, Grant NE, Kwaplil W, Murphy JD, Schubert MC. Light-induced activation and deactivation of bulk defects in boron-doped float-zone silicon. *J Appl Phys*. 2017;121(18):185702.
 39. Petter K, Hubener K, Kersten F, et al. Dependence of LeTID on brick height for different wafer suppliers with several resistivities and dopants. *9th Int Work Cryst Silicon Sol Cells*. 2016;6(4):1-17.
 40. Jensen MA, Morishige AE, Hofstetter J, Needleman DB, Buonassisi T. Evolution of LeTID defects in p-type multicrystalline silicon during degradation and regeneration. *IEEE J Photovoltaics*. 2017;7(4):980-987.
 41. Chan C, Fung TH, Abbott M, et al. Modulation of carrier-induced defect kinetics in multi-crystalline silicon PERC cells through dark annealing. *Sol RRL*. 2017;1(2):1600028.
 42. Hallam B, Chen D, Kim M, et al. The role of hydrogenation and gettering in enhancing the efficiency of next-generation Si solar cells: an industrial perspective. *Phys status solidi*. 2017;214(7):1700305.
 43. Talvitie H, Vähäniemi V, Haarhiltunen A, Yli-Koski M, Savin H. Phosphorus and boron diffusion gettering of iron in monocrystalline silicon. *J Appl Phys*. 2011;109(9):093505.
 44. Chen D, Edwards M, Wenham S, Abbott M, Hallam B. Laser enhanced gettering of silicon substrates. *Front Energy*. 2017;11(1):23-31.
 45. Hallam BJ, Hamer PG, Wenham SR, et al. Advanced bulk defect passivation for silicon solar cells. *IEEE J Photovoltaics*. 2014;4(1):88-95.
 46. Lee SH, Bhopal MF, Lee DW, Lee SH. Review of advanced hydrogen passivation for high efficient crystalline silicon solar cells. *Mater Sci Semicond Process*. 2018;79(January):66-73.
 47. Martinuzzi S, Péricaud I, Warchol F. Hydrogen passivation of defects in multicrystalline silicon solar cells. *Sol Energy Mater Sol Cells*. 2003;80(3):343-353.
 48. Hallam BJ, Hamer PG, Wang S, et al. Advanced hydrogenation of dislocation clusters and boron-oxygen defects in silicon solar cells. *Energy Procedia*. 2015;77:799-809.
 49. Hamer P, Hallam B, Wenham S, Abbott M. Manipulation of hydrogen charge states for passivation of P-type wafers in photovoltaics. *IEEE J Photovoltaics*. 2014;4(5):1252-1260.
 50. Herguth A, Schubert G, Kaes M, Hahn G. Avoiding boron-oxygen related degradation in highly boron doped Cz silicon. *Proc 21st Eur Photovolt Sol Energy Conf*. 2006;530-537.
 51. Hallam BJ, Chan CE, Chen R, et al. Rapid mitigation of carrier-induced degradation in commercial silicon solar cells. *Jpn J Appl Phys*. 2017;56(8S2):08MB13.
 52. Helmich L, Walter DC, Bredemeier D, Falster R, Voronkov VV, Schmidt J. In-situ characterisation of electron-assisted regeneration of Cz-Si solar cells. *Sol Energy Mater Sol Cells*. 2018;185(October):283-286.
 53. Herguth A, Hahn G. Boron-oxygen related defects in Cz-silicon solar cells degradation, regeneration and beyond. 2009;2(September):974-976.
 54. Hallam BJ, Wenham SR, Hamer PG, et al. Hydrogen passivation of B-O defects in Czochralski silicon. *Energy Procedia*. 2013;38:561-570.
 55. Hamer P, Hallam B, Abbott M, Wenham S. Accelerated formation of the boron-oxygen complex in p-type Czochralski silicon. *Phys Status Solidi Rapid Res Lett*. 2015;9(5):297-300.
 56. Heiser T, Mesli A. How far does the charge state affect the iron behavior in silicon? *Appl Phys Lett*. 1991;58(20):2240-2242.
 57. Heiser T, Mesli A. Charge-state-dependent diffusion and carrier-emission-limited drift of iron in silicon. *Phys Rev Lett*. 1992;68(7):978-981.
 58. Gilles D, Schröter W, Bergholz W. Impact of the electronic structure on the solubility and diffusion of 3d transition elements in silicon. *Phys Rev B*. 1990;41(9):5770-5782.
 59. Kovoshnikov SV, Rozgonyi GA. Iron diffusivity in silicon: impact of charge state. *Appl Phys Lett*. 1995;66(7):860-862.
 60. Mesli A, Heiser T, Amroun N, Siffert P. Charge-state-dependent iron precipitation in silicon. *Appl Phys Lett*. 1990;57(18):1898-1900.
 61. Nakashima, K., and Chijiwa, M. (1986) Optical and thermal ionization of iron-related defects in silicon. *Jpn J Appl Phys*, 25 (Part 1, No. 2), 234-237.
 62. Schwalbach P, Laubach S, Hartick M, et al. Diffusion and isomer shift of interstitial iron in silicon observed via in-beam Mössbauer spectroscopy. *Phys Rev Lett*. 1990;64(11):1274-1277.
 63. Shepherd WH, Turner JA. Iron-boron pairing in silicon. *J Phys Chem Solid*. 1962;23(12):1697-1706.
 64. Struthers JD. Solubility and diffusivity of gold, iron, and copper in silicon. *J Appl Phys*. 1956;27(12):1560-1560.
 65. Isobe, T., Nakashima, H., and Hashimoto, K. (1989) Diffusion coefficient of interstitial iron in silicon. *Jpn J Appl Phys*, 28 (Part 1, No. 7), 1282-1283.
 66. Wijaranakula W. The reaction kinetics of iron-boron pair formation and dissociation in p-type silicon. *J Electrochem Soc*. 1993;140(1):275.
 67. Istratov AA, Hieslmair H, Weber ER. Iron and its complexes in silicon. *Appl Phys A Mater Sci Process*. 1999;44:13-44.
 68. Kleekajai S, Jiang F, Stavola M, et al. Concentration and penetration depth of H introduced into crystalline Si by hydrogenation methods used to fabricate solar cells. *J Appl Phys*. 2006;100(9):093517.
 69. Huang YL, Ma Y, Job R, Ulyashin AG. Hydrogen diffusion at moderate temperatures in p-type Czochralski silicon. *J Appl Phys*. 2004;96(12):7080-7086.
 70. Johnson NM, Herring C. Hydrogen migration and complex-formation in silicon. *Inst Phys Conf Ser*. 1989;415-424.
 71. Johnson NM, Moyer MD. Absence of oxygen diffusion during hydrogen passivation of shallow-acceptor impurities in single-crystal silicon. *Appl Phys Lett*. 1985;46(8):787-789.
 72. Newman RC, Tucker JH, Brown AR, McQuaid SA. Hydrogen diffusion and the catalysis of enhanced oxygen diffusion in silicon at temperatures below 500 °C. *J Appl Phys*. 1991;70(6):3061-3070.
 73. Pearton SJ. Hydrogen in crystalline silicon. *Mat Res Soc Symp Proc*. 1985;59:457-468.
 74. Stavola M, Jiang F, Rohatgi A, et al. Hydrogenation of Si from SiNx: H films: how much hydrogen is really in the Si? *Proc 3rd World Conf Photovolt Energy Conversion, Vols a-C*. 2003;1:909-912.
 75. Capizzi M, Mittiga A. Hydrogen in crystalline silicon: a deep donor. *Appl Phys Lett*. 1987;50(14):918-920.
 76. Hansen WL, Pearton SJ, Haller EE. Bulk acceptor compensation produced in p-type silicon at near-ambient temperatures by a H2O plasma. *Appl Phys Lett*. 1984;44(6):606-608.
 77. Ichimiya T, Furuchi A. On the solubility and diffusion coefficient of tritium in single crystals of silicon. *Int J Appl Radiat Isot*. 1968;19(7):573-578.
 78. Mogro-Campero A. Drastic changes in the electrical resistance of gold-doped silicon produced by a hydrogen plasma. *J Electrochem Soc*. 1985;132(8):2006.
 79. Seager CH, Anderson RA. Electronic control of hydrogen debonding from phosphorus in silicon—is there an acceptor state of interstitial hydrogen? *Solid State Commun*. 1990;76(3):285-288.
 80. Seager CH, Anderson RA. Real-time observations of hydrogen drift and diffusion in silicon. *Appl Phys Lett*. 1988;53(13):1181-1183.
 81. Sopori BL, Jones K, Deng XJ. Observation of enhanced hydrogen diffusion in solar cell silicon. *Appl Phys Lett*. 1992;61(21):2560-2562.
 82. Van Wieringen A, Warmoltz N. On the permeation of hydrogen and helium in single crystal silicon and germanium at elevated temperatures. *Phys Ther*. 1956;22(6-12):849-865.

83. Mathiot D. Modeling of hydrogen diffusion in n-and p-type silicon. *Phys Rev B*. 1989;40(8):5867-5870.
84. Sun C, Rougiew F, Macdonald D. A unified approach to modelling the charge state of monatomic hydrogen and other defects in crystalline silicon. *J Appl Phys*. 2015;117(4):045702.
85. Zundel T, Weber J. Trap-limited hydrogen diffusion in boron-doped silicon. *Phys Rev B*. 1992;46(4):2071-2077.
86. Herrero CP, Stutzmann M, Breitschwerdt A, Santos PV. Trap-limited hydrogen diffusion in doped silicon. *Phys Rev B*. 1990;41(2):1054-1058.
87. Dubé C, Hanoka JI, Sandstrom DB. Hydrogen diffusion along passivated grain boundaries in silicon ribbon. *Appl Phys Lett*. 1984;44(4):425-427.
88. Park H, Tark SJ, Kim CS, et al. Effect of the phosphorus gettering on Si heterojunction solar cells. *Int J Photoenergy*. 2012;2012:1-7.
89. Hallam B, Chen D, Shi J, Einhaus R, Holman ZC, Wenham S. Prefabrication gettering and hydrogenation treatments for silicon heterojunction solar cells: a possible path to >700 mV open-circuit voltages using low-lifetime commercial-grade p-type Czochralski silicon. *Sol RRL*. 2018;2(2):1700221.
90. Basnet, R., Weigand, W., Yu, Z.J., Sun, C., Phang, S.P., Rougiew, F.E., Einhaus, R., Degoulange, J., Holman, Z., and Macdonald, D. (2018) Impact of tabula rasa and phosphorus diffusion gettering on 21% heterojunction solar cells based on n-type czochralski-grown upgrade metallurgical-grade silicon. 2018 IEEE 7th World Conf. Photovolt. Energy Conversion, WCPEC 2018 - A Jt. Conf. 45th IEEE PVSC, 28th PVSEC 34th EU PVSEC, 1687-1691.
91. Haschke, J., Kivambe, M.M., Horzel, J., Monnard, R., Barraud, L., Descoedres, A., Debrot, F., Abdallah, A., Aissa, B., Tabet, N., Despeisse, M., Boccard, M., and Ballif, C. (2018) Silicon heterojunction solar cells on quasi-mono wafers. 2018 IEEE 7th World Conf. Photovolt. Energy Conversion, WCPEC 2018 - A Jt. Conf. 45th IEEE PVSC, 28th PVSEC 34th EU PVSEC, 314-316.
92. Shi J, Boccard M, Holman Z. Plasma-initiated rehydrogenation of amorphous silicon to increase the temperature processing window of silicon heterojunction solar cells. *Appl Phys Lett*. 2016;109(3):031601.
93. Descoedres A, Barraud L, De Wolf S, et al. Improved amorphous-crystalline silicon interface passivation by hydrogen plasma treatment. *Appl Phys Lett*. 2011;99(12):123506.
94. Payne DNR, Chan CE, Hallam BJ, et al. Acceleration and mitigation of carrier-induced degradation in p-type multi-crystalline silicon. *Phys Status Solidi Rapid Res Lett*. 2016;10(3):237-241.
95. Sinton, R.A., Cuevas, A., and Stuckings, M. (1996) Quasi-steady-state photoconductance, a new method for solar cell material and device characterization. *Conf. Rec. Twenty Fifth IEEE Photovolt. Spec. Conf.* - 1996.
96. Nagel H, Berge C, Aberle AG. Generalized analysis of quasi-steady-state and quasi-transient measurements of carrier lifetimes in semiconductors. *J Appl Phys*. 1999;86(11):6218-6221.
97. Richter A, Werner F, Cuevas A, Schmidt J, Glunz SW. Improved parameterization of auger recombination in silicon. *Energy Procedia*. 2012;27:88-94.
98. Naerland TU, Haug H, Angelskar H, Sondena R, Marstein ES, Arnberg L. Studying light-induced degradation by lifetime decay analysis: excellent fit to solution of simple second-order rate equation. *IEEE J Photovoltaics*. 2013;3(4):1265-1270.
99. Kane D, Richard S. Measurement of the emitter saturation current by a contactless photoconductivity decay method. *IEEE Photovolt Spec Conf*. 1985;578-583.
100. Cuevas A, Macdonald D. Measuring and interpreting the lifetime of silicon wafers. *Sol Energy*. 2004;76(1-3):255-262.
101. Macdonald D, Roth T, Deenapanray PNK, Bothe K, Pohl P, Schmidt J. Formation rates of iron-acceptor pairs in crystalline silicon. *J Appl Phys*. 2005;98(8):083509.
102. Hallam B, Tjahjono B, Trupke T, Wenham S. Photoluminescence imaging for determining the spatially resolved implied open circuit voltage of silicon solar cells. *J Appl Phys*. 2014;115(4):044901.
103. Teal, A., and Juhl, M. (2015) Correcting the inherent distortion in luminescence images of silicon solar cells. 2015 IEEE 42nd Photovolt. Spec. Conf., 1-5.
104. Payne DNR, Vargas C, Hameiri Z, Wenham SR, Bagnall DM. An advanced software suite for the processing and analysis of silicon luminescence images. *Comput Phys Commun*. 2017;215:223-234.
105. Liu AY, Sun C, Markevich VP, Peaker AR, Murphy JD, Macdonald D. Gettering of interstitial iron in silicon by plasma-enhanced chemical vapour deposited silicon nitride films. *J Appl Phys*. 2016;120(19):193103.
106. Azzizi, A., Geerligs, L.J., and Macdonald, D. (2004) Hydrogen passivation of iron in crystalline silicon. 19th EUPVSEC.
107. Liu A, Sun C, MacDonald D. Hydrogen passivation of interstitial iron in boron-doped multicrystalline silicon during annealing. *J Appl Phys*. 2014;116(19):0-10.
108. Lelièvre JF, Hofstetter J, Peral A, Hoces I, Recart F, Del Cañizo C. Dissolution and gettering of iron during contact co-firing. *Energy Procedia*. 2011;8(April):257-262.
109. Deng W, Ye F, Liu R, Li Y, Chen H, Xiong Z, Yang Y, Chen Y, Wang Y, Altermatt P.P., Feng Z, and Verlinden P.J. (2017) 22.61% Efficient fully screen printed PERC solar cell. 2017 IEEE 44th Photovolt. Spec. Conf., 1-4.
110. Kobayashi E, De Wolf S, Levrat J, et al. Light-induced performance increase of silicon heterojunction solar cells. *Appl Phys Lett*. 2016;109(15):153503.
111. Kobayashi E, De Wolf S, Levrat J, et al. Increasing the efficiency of silicon heterojunction solar cells and modules by light soaking. *Sol Energy Mater Sol Cells*. 2017;173:43-49.
112. Descoedres A, Holman ZC, Barraud L, Morel S, De Wolf S, Ballif C. 21% Efficient silicon heterojunction solar cells on n- and p-type wafers compared. *IEEE J Photovoltaics*. 2013;3(1):83-89.
113. Olibet S, Vallat-Sauvain E, Ballif C. Model for a-Si:H/c-Si interface recombination based on the amphoteric nature of silicon dangling bonds. *Phys Rev B*. 2007;76(3):035326.
114. Iuliis, S., and Geerligs, B. (2007) Response of n-type mc-Si to large variations of gettering and hydrogenation. 17 th Work. Cryst. Silicon Sol. Cells Modul. Mater. Process., 298.
115. Benick, J., Müller, R., Schindler, F., Richter, A., Hauser, H., Feldmann, F., Krenckel, P., Riepe, S., Schubert, M., Hermle, M., and Glunz, S.W. (2017) Approaching 22% efficiency with multicrystalline n-type silicon solar cells. 33rd Eur. Photovolt. Sol. Energy Conf. Exhib. EU PVSEC 2017, (September), 460-464.
116. Sun C, Chen D, Rougiew F, Basnet R, Hallam B, Macdonald D. Kinetics and dynamics of the regeneration of boron-oxygen defects in compensated n-type silicon. *Sol Energy Mater Sol Cells*. 2019;195 (2019):174-181.
117. Sun, C., Weigand, W., Chen, D., Holman, Z.C., Basnet, R., Yu, Z. (Jason), Phang, S.P., Hallam, B., and Macdonald, D. (2019) Key structures in silicon heterojunction solar cells for the complete regeneration of BO-related defects in n-type upgraded metallurgical-grade Czochralski silicon. 36th Eur. Photovolt. Sol. Energy Conf. Exhib.
118. Sperber, D., Herguth, A., and Hahn, G. (2017) Investigating possible causes of light induced degradation in boron-doped float-zone silicon. *Proc. 33rd EUPVSEC*, 565-568.
119. Fung TH, Kim M, Chen D, et al. A four-state kinetic model for the carrier-induced degradation in multicrystalline silicon: introducing the reservoir state. *Sol Energy Mater Sol Cells*. 2018;184:48-56.
120. Eberle R, Kwapił W, Schindler F, Schubert MC, Glunz SW. Impact of the firing temperature profile on light induced degradation of multicrystalline silicon. *Phys Status Solidi Rapid Res Lett*. 2016;865(12):861-865.

121. Vargas C, Zhu Y, Coletti G, et al. Recombination parameters of lifetime-limiting carrier-induced defects in multicrystalline silicon for solar cells. *Appl Phys Lett.* 2017;110(9):092106.
122. Morishige AE, Jensen MA, Needleman DB, et al. Lifetime spectroscopy investigation of light-induced degradation in p-type multicrystalline silicon PERC. *IEEE J Photovoltaics.* 2016;6(6):1466-1472.
123. Bredemeier, D., Walter, D., Herlufsen, S., and Schmidt, J. (2016) Understanding the light-induced lifetime degradation and regeneration in multicrystalline silicon. *Energy Procedia*, 92 (0), 773-778.
124. Bredemeier D, Walter D, Herlufsen S, Schmidt J. Lifetime degradation and regeneration in multicrystalline silicon under illumination at elevated temperature. *AIP Adv.* 2016;6(3):035119.
125. Chan CE, Payne DNR, Hallam BJ, et al. Rapid stabilization of high-performance multicrystalline p-type silicon PERC cells. *IEEE J Photovoltaics.* 2016;6(6):1473-1479.

How to cite this article: Chen D, Kim M, Shi J, et al. Defect engineering of p-type silicon heterojunction solar cells fabricated using commercial-grade low-lifetime silicon wafers. *Prog Photovolt Res Appl.* 2021;29(11):1165-1179. <https://doi.org/10.1002/pip.3230>